Alzheimer's & Dementia 15 (2019) 1172-1182

Featured Article

^{18}F-FDG PET, the early phases and the delivery rate of ^{18}F-AV45 PET as proxies of cerebral blood flow in Alzheimer's disease: Validation against ^{15}O-H_2O PET

Julie Ottoy[a], Jeroen Verhaeghe[a], Ellis Niemantsverdriet[b], Ellen De Roeck[b], Leonie wyffels[c], Sarah Ceyssens[c], Christine Van Broeckhoven[d,e], Sebastiaan Engelborghs[b,f], Sigrid Stroobants[c], Steven Staelens[a,*]

[a]*Molecular Imaging Centre Antwerp, University of Antwerp, Antwerp, Belgium*
[b]*Reference Centre for Biological Markers of Dementia (BIODEM), Laboratory of Neurochemistry and Behaviour, Institute Born-Bunge, University of Antwerp, Antwerp, Belgium*
[c]*Department of Nuclear Medicine, Antwerp University Hospital, Edegem, Belgium*
[d]*Neurodegenerative Brain Diseases Group, Centre for Molecular Neurology, VIB, Antwerp, Belgium*
[e]*Laboratory of Neurogenetics, Institute Born-Bunge, University of Antwerp, Antwerp, Belgium*
[f]*Department of Neurology and Memory Clinic, Hospital Network Antwerp (ZNA) Middelheim and Hoge Beuken, Antwerp, Belgium*

Abstract

Introduction: Dual-biomarker positron emission tomography (PET), providing complementary information on cerebral blood flow and amyloid-β deposition, is of clinical interest for Alzheimer's disease (AD). The purpose of this study was to validate the perfusion components of early-phase ^{18}F-florbetapir (eAV45), the ^{18}F-AV45 delivery rate (R1), and ^{18}F-FDG against ^{15}O-H_2O PET and assess how they change with disease severity.

Methods: This study included ten controls, 19 amnestic mild cognitive impairment, and 10 AD dementia subjects. Within-subject regional correlations between modalities, between-group regional and voxel-wise analyses of covariance per modality, and receiver operating characteristic analyses for discrimination between groups were performed.

Results: FDG standardized uptake value ratio, eAV45 (0–2 min) standardized uptake value ratio, and AV45-R1 were significantly associated with H_2O PET (regional Pearson r = 0.54–0.82, 0.70–0.94, and 0.65–0.92, respectively; $P < .001$). All modalities confirmed reduced cerebral blood flow in the posterior cingulate of patients with amnestic mild cognitive impairment and AD dementia, which was associated with lower cognition (r = 0.36–0.65, $P < .025$) and could discriminate between patient and control groups (area under the curve > 0.80). However, eAV45 was less sensitive to reflect the disease severity than AV45-R1 or FDG.

Discussion: R1 is preferable over eAV45 for accurate representation of brain perfusion in dual-biomarker PET for AD.

Keywords: Alzheimer's disease; Cerebral blood flow; Dual-phase PET; Early-phase PET; ^{18}F-AV45; ^{18}F-FDG; ^{15}O-H_2O; Perfusion imaging; R1

1. Introduction

Alzheimer's disease (AD) is a progressive, neurodegenerative disorder characterized by the presence of intracellular neurofibrillary tangles and extracellular amyloid-β (Aβ)

The authors have declared that no conflict of interest exists.

*Corresponding author. Tel.: +32-32652820; Fax: +32-32652813.
E-mail address: steven.staelens@uantwerpen.be

https://doi.org/10.1016/j.jalz.2019.05.010

plaques in the brain [1]. These protein aggregates cause neuropathological changes, leading to synaptic and neuronal cell death, as well as progressive loss of cognitive function. While the accumulation of Aβ plaques is believed to be one of the factors driving AD pathogenesis and is used for diagnostic workup, there is evidence that also vascular and metabolic factors are involved in the development and progression of AD [2]. Indeed, prior imaging studies have demonstrated brain patterns of reduced cerebral blood flow (CBF) and cerebral metabolic rates of glucose (CMRglc) as possible biomarkers of AD [3,4]. Moreover, these markers were found to be particularly sensitive in predicting cognitive decline and conversion to AD dementia; therefore, they can be applied to identify clinical drug trial participants who are in a milder and earlier phase of the disease [5,6]. In addition, because of their direct relationship with symptom severity, CBF and CMRglc patterns may be used to assess a therapeutic response in these trials [7,8].

The ^{15}O-H_2O tissue concentration is known to be linearly related to CBF [9]. Hence, the gold standard for noninvasive measurement of CBF is ^{15}O-labeled H_2O positron emission tomography (PET). However, the short decay time of ^{15}O limits its use in routine clinical practice and to sites with a cyclotron. Recent work has shown that the early time frames of dynamic ^{11}C-Pittsburgh compound B (PiB) PET are closely related to the first-pass influx rate (K1), the latter being strongly correlated to CBF because of a high extraction fraction of lipophilic radiotracers into the brain (K1 = CBF × extraction, with extraction ≈ 77% for ^{11}C-PiB) [10,11]. This is of clinical interest as perfusion may be derived from the earliest frames of the PET scan, whereas Aβ burden can be measured at later times after injection, thereby combining functional and pathological information in one Aβ-tracer PET protocol [12]. Alternatively, the ratio of K1 to its reference region value (i.e., delivery rate R1), serving as a measure of relative perfusion, can be derived together with the amyloid binding potential (BP_{ND}) from pharmacokinetic modeling of one dynamic amyloid-PET scan [13]. Our group previously validated the R1 of ^{18}F-florbetapir (^{18}F-AV45) against the standardized uptake value ratio (SUVR) of ^{15}O-H_2O PET in the AD spectrum [14]. Indeed, ^{18}F-AV45 is known to be lipophilic (Moriguchi logP 2.52 [15]) and thus to have good extraction into the brain. However, R1 was based on dynamic scanning with arterial cannulation and labor-intensive metabolite analysis. No studies have yet validated ^{18}F-AV45-R1 based on the (two-step) simplified reference tissue model (SRTM2) [16] or the early phases of ^{18}F-AV45 (^{18}F-eAV45) against ^{15}O-H_2O PET.

Both R1 and the early phases of amyloid-PET have also shown good correlations to ^{18}F-fluorodeoxyglucose (^{18}F-FDG) uptake, suggesting their potential use as biomarkers of neuronal dysfunction [12,17–23]. A dual-biomarker scan may thus provide information on both Aβ pathology and neuronal injury/neurodegeneration and ultimately circumvent the need for an additional ^{18}F-FDG scan in the dementia workup [21]. Such an approach would be highly useful in the clinic as it results in decreased costs, less radiation exposure, and more patient comfort [12,24]. In this study, we investigated the association between CBF and CMRglc distribution by comparing ^{18}F-FDG PET directly to ^{15}O-H_2O PET in sporadic AD and how these markers associate with cognition.

In conclusion, the main objectives of this work were three-fold: (1) determine the optimal early time frame of ^{18}F-eAV45 in association with ^{15}O-H_2O PET; (2) evaluate the perfusion components of ^{18}F-eAV45, SRTM2-based R1, and ^{18}F-FDG in comparison to ^{15}O-H_2O data; and (3) investigate how these measures relate with clinical diagnosis and cognition. All analyses investigated the impact of the most widely used reference regions for these tracers: cerebellar gray matter (CB) and pons for ^{18}F-FDG quantification, and CB and subcortical white matter (WM) for ^{18}F-AV45 quantification.

2. Methods

2.1. Study population

Thirty-nine subjects were enrolled in the study, including 10 healthy controls (HCs), 19 amnestic mild cognitive impairment (aMCI) subjects, and 10 AD dementia subjects. Their demographics are shown in Table 1. All subjects underwent ^{18}F-AV45 (AV45) PET, ^{18}F-FDG (FDG) PET, ^{15}O-H_2O (H_2O) PET, magnetic resonance imaging (MRI), and a neuropsychological examination, including the Mini-Mental State Examination (MMSE) and the Repeatable Battery for the Assessment of Neuropsychological Status composed of the immediate and delayed memory index scores [25]. Categorization into diagnostic groups was made on a demographical and clinical basis by obtaining consensus from three expert medical doctors. Clinical diagnoses of "MCI due to AD" (MCI) and "dementia due to AD" (AD dementia) were based on the criteria of the National Institute on Aging and Alzheimer's Association [26,27]. A description of inclusion and exclusion criteria can be found in the study by Niemantsverdriet et al. [28]. Patients were recruited through the Memory Clinic of ZNA Middelheim and Hoge Beuken, Antwerp, Belgium. Cognitively healthy elderly consisted of volunteers, mainly spouses of patients who visited the memory clinic.

Approval for the study was obtained from the Committee for Medical Ethics of the University of Antwerp/University Hospital Antwerp (14/12/130) and of Hospital Network Antwerp (ZNA) (4310), and all procedures were performed in accordance with the Helsinki Declaration of 1975. All participants or their representatives provided written informed consent.

2.2. Image acquisition and analysis

Procedures for acquisition of PET and magnetic resonance images and radiometabolite analysis are described elsewhere [14]. Briefly, 3D T1-weighted magnetization-prepared rapid acquisition gradient-echo scans were obtained on a Siemens Trio Tim 3T magnetic resonance scanner with

Table 1
Demographics

Characteristics	HC (n = 10)	aMCI (n = 19)	AD dementia (n = 10)
Female gender, %	60	47	30
Age, years	69 ± 6	73 ± 8	73 ± 5
Education, years	19 ± 3	15 ± 5*	15 ± 4
APOE ε4 carriers, % (n)	50 (4/8)	77 (13/17)	67 (6/9)
MMSE	29 ± 1	25 ± 3*	22 ± 4*
Cortical $SUVR_{WM}$ (%Aβ+)	0.57 ± 0.2 (40)	0.79 ± 0.2* (89)	0.83 ± 0.1* (100)

NOTE. Data presented as mean ± standard deviation. The Aβ cutoff was determined previously in the study by Niemantsverdriet et al. [28].

Abbreviations: Aβ, amyloid β; AD, Alzheimer's disease; aMCI, amnestic mild cognitive impairment; *APOE* ε4, apolipoprotein ε4 allele; HC, healthy controls; MMSE, Mini-Mental State Examination; SUVR, standardized uptake value ratio.

*$P < .05$ versus HC subjects. Categorical variables (gender, *APOE* ε4) via Fisher's exact test; continuous variables (age, education, MMSE, SUVR) via Kruskal-Wallis corrected for multiple comparisons via Bonferroni.

1-mm isotropic voxels. ^{18}F-AV45 was injected as an intravenous bolus of 291 ± 66 MBq, and 60-min dynamic scanning was performed on a Siemens Biograph mCT time-of-flight PET scanner. Simultaneously with the dynamic AV45 PET acquisition, 60-min continuous arterial blood sampling (Twilite; Swisstrace, Switzerland) and manual sampling at discrete time points was performed to derive the metabolite-corrected plasma input function for each subject. Time-weighted averaging of the early frames of the dynamic AV45 scans between the start time (T1 = 0, 30, or 60 s) and end time (T2 = 1, 2, 3, 4, or 6 min) after injection was performed in PMOD (PMOD Technologies Ltd., Zurich, Switzerland) to generate an array of potential eAV45 images. The time-weighted averaging method was first validated against the reconstruction of the list-mode AV45 dynamic data into a single frame. For the first 6 min of AV45, correlations between resulting SUVRs of both methods were as high as 0.99 (Pearson r). Therefore, the time-weighted averaging method was used to determine eAV45 images in this manuscript. Dynamic H_2O (370 MBq) and static FDG (153 ± 18 MBq) images were acquired at 0–2 min and 30–40 min after injection, respectively. Time interval between PET acquisitions within one subject was minimal (AV45 vs. H_2O: 24 ± 180 days, vs. FDG: 24 ± 181 days, vs. MRI: 22 ± 77 days).

Interframe motion correction of the dynamic PET scans and PET-to-MRI coregistration were performed for each subject separately using PMOD v3.6 (PMOD Technologies Ltd., Zurich, Switzerland). The eAV45 and R1 PET-to-MRI coregistration was based on the first 2-min and the 60-min data, respectively. Regions of interest (ROIs) were delineated using automated knowledge-based "gray matter/WM/cerebrospinal fluid" segmentation of each subject's MRI and the Automated Anatomical Labeling atlas in PMOD. ROIs included the cortical gray matter target regions (the four cortical lobes, anterior cingulate cortex, posterior cingulate cortex [PCC], precuneus), the hippocampus target region, and the reference regions CB, whole subcortical WM, and pons. PET time-activity curves were extracted in the different ROIs and corrected for partial volume effects based on the region-based geometric transfer matrix method [29] and a 5 × 5 × 5-mm^3 PET scanner resolution. Regional H_2O, eAV45, and FDG were quantified as SUVR at 0–1 min, T1-T2 min, and 30–40 min after injection, respectively. Regional R1 values were derived from 2-tissue compartment modeling (2TCM4k_Vb) of the dynamic AV45 images and metabolite-corrected plasma input functions [14]. Alternatively, R1 was computed based on SRTM2 with fixed k2' using a coupled fit across the target ROIs. SRTM2 was chosen over SRTM as the former model has been shown to reduce noise [16]. The CB and pons were applied as reference regions for FDG SUVR, whereas CB and WM were applied as reference regions for eAV45 SUVR and R1. H_2O SUVR was considered as the gold standard to measure CBF using CB, pons, or WM as the reference region.

Voxel-wise AV45-R1 maps were generated using PXMOD v3.3 with SRTM2 and a fixed subject-specific k2' extracted from the regional kinetic modeling toolbox (PKIN). All CBF maps were normalized and averaged per tracer and diagnostic group to compare their spatial patterns.

2.3. Statistical analysis

Statistical analyses were performed in IBM SPSS Statistics v24. Demographical differences among diagnostic groups were assessed using Fisher's exact tests for categorical variables and Kruskal-Wallis tests with Bonferroni correction for continuous variables. The optimal early time frame of eAV45 was determined when the highest correlation (Pearson r) between eAV45 (T1,T2) and H_2O SUVRs was achieved. Furthermore, Pearson r was used to assess correlations between all CBF measures, as well as to assess partial correlations between CBF and cognitive scores corrected for age and education. All correlative analyses were corrected for multiple comparisons (number of ROIs) using Bonferroni at $P < .05$, .01, .001, and .0001 and included all subjects. To compare differences in CBF patterns between the diagnostic groups, voxel-wise analyses of covariance ($P < .05$ corrected for age and education, cluster extent ≥ 50 voxels) were performed in SPM12 (Wellcome Department of Cognitive Neurology, London, UK) implemented in MATLAB 2017 (The Mathworks, Sherborn, MA, USA). Finally, receiver operating characteristic area under the curve (AUC) analyses were applied on regional CBF measures to compare their discriminative ability for classification of patients with aMCI/AD dementia from HCs.

3. Results

3.1. Reference regions

The SUV and K1 values of the pons, CB, and WM—representing the blood flow in the reference regions—did

not significantly differ between the diagnostic groups (Supplementary Table 1). Within one CBF measure and diagnostic group, the coefficient of variation was similar across reference regions.

3.2. Validation of SRTM2-based R1

The AV45 delivery rate R1 derived from the 2TCM was strongly correlated with R1 from SRTM2. For reference CB, correlation coefficients were as high as 0.98 – 0.99 ($P < .0001$) in the target regions, except for the PCC (r = 0.94, $P < .0001$). For reference WM, correlation coefficients were slightly lower, ranging from 0.78 in the temporal lobe to 0.95 in the PCC and hippocampus ($P < .0001$). R1 based on the SRTM2 was used in all further analyses.

3.3. Optimization of early time frame of eAV45

To optimize the early time frame for eAV45, correlation plots of different early time frames of AV45 (start time T1 = 0, 30, or 60 s; end time T2 = 1, 2, 3, 4, or 6 min) versus H_2O SUVR (and for completeness, vs. AV45-R1 as well) are shown in Fig. 1. Pearson r was highest when the time frame of 0–2 min was selected for eAV45. Excluding the first 30 s from the early phases (black curves) gave similar results as starting at 0 s; however, excluding the first 60 s resulted in lower correlation coefficients (red curves). As a result, eAV45 (0–2 min) was used in further analyses as a proxy of CBF.

3.4. CBF proxies versus H_2O PET

Among all relative CBF proxies, the early-phase $SUVR_{CB}$ and $R1_{CB}$ of AV45 were most strongly correlated to the gold standard H_2O $SUVR_{CB}$ (Pearson r ranging from 0.83 [occipital lobe] and 0.78 [hippocampus], respectively, to 0.94 and 0.92 [temporal lobe], respectively; $P < .00001$) (Table 2). For WM reference, these regional correlations performed slightly weaker (Pearson r ranging from 0.70 and 0.65 [hippocampus], respectively, to 0.86 [precuneus] and 0.84 [PCC], respectively; $P < .00001$). FDG SUVR performed the weakest of all measures in relation to H_2O SUVR, notably in the frontal and occipital lobe and hippocampus (Pearson r < 0.7, $P < .001$). When stratifying per diagnostic group, similar relationships between the different modalities were found, and all CBF proxies overestimated H_2O SUVR (Supplementary Fig. 1).

Absolute measures representing global CBF showed, in general, weak correlations with H_2O SUV (Pearson r < 0.7) (Table 2). Correlations of H_2O SUV with the AV45 delivery rate K1 reached significance in all regions (Pearson r ranging from 0.44 in the parietal lobe to 0.68 in the PCC, $P < .006$), whereas correlations with FDG SUV were significant only in the precuneus and PCC (r = 0.44 and 0.45, respectively, $P < .006$). eAV45 and H_2O SUV were significantly correlated only in the PCC (r = 0.54, $P < .001$).

3.5. CBF versus clinical diagnosis and cognition

Group-averaged images of the four CBF proxies normalized to CB are shown in Fig. 2; group-averaged images with

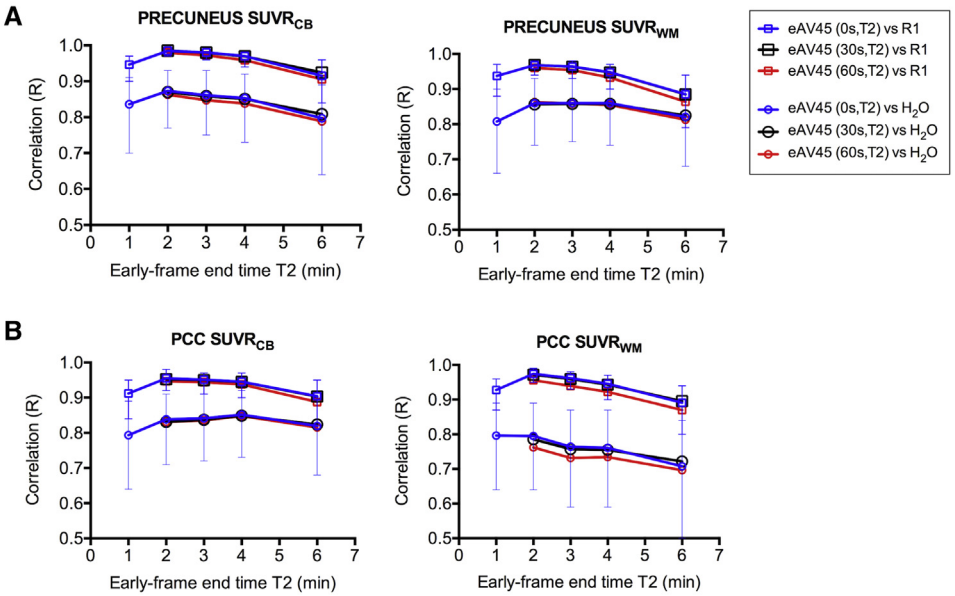

Fig. 1. Within-subject correlations of early-phase AV45 SUVR with H_2O SUVR (circles) and AV45-R1 (squares) using the precuneus (A) or the PCC (B) as the target region and the CB (left) or the WM (right) as the reference region. The early-phase time frames were T1 and T2, with T1 being 0, 30, or 60 sec (blue, black, and red curves, respectively) and T2 being 1, 2, 3, 4, or 6 min (X-axis). For the blue curves, the 95% confidence intervals of the correlations are shown as well. Abbreviations: eAV45, early-phase AV45; PCC, posterior cingulate cortex; SUVR, standardized uptake value ratio.

Table 2
ROI-based within-subject correlation (Pearson r) of H_2O with FDG, early-phase AV45, and the AV45 delivery rate

	H_2O vs. FDG			H_2O vs. eAV45			H_2O vs. AV45 K1/R1		
		Relative (SUVR)			Relative (SUVR)		Absolute	Relative (SUVR/R1)	
ROI	Absolute (SUV)	CB	Pons	Absolute (SUV)	CB	WM	(SUV/K1)	CB	WM
Frontal lobe	0.37	0.65§	0.57†	0.35	0.90§	0.81§	0.46*	0.91§	0.76§
Parietal lobe	0.36	0.73§	0.73§	0.38	0.89§	0.84§	0.44*	0.88§	0.80§
Temporal lobe	0.41	0.82§	0.75§	0.39	0.94§	0.83§	0.51†	0.92§	0.83§
Occipital lobe	0.25	0.57†	0.54†	0.33	0.83§	0.82§	0.47*	0.82§	0.78§
Precuneus	0.44*	0.72§	0.79§	0.36	0.87§	0.86§	0.54†	0.87§	0.81§
Hippocampus	0.29	0.55†	0.62‡	0.38	0.85§	0.70§	0.50*	0.78§	0.65§
ACC	0.32	0.80§	0.70§	0.36	0.89§	0.79§	0.55†	0.89§	0.78§
PCC	0.45*	0.75§	0.76§	0.54†	0.84§	0.80§	0.68§	0.89§	0.84§

NOTE. For the relative measures, CB, pons, and WM were investigated as reference regions.

Abbreviations: ACC, anterior cingulate cortex; CB, cerebellar gray matter; eAV45, early-phase AV45; K1 (or R1), AV45 (relative) delivery rate; PCC, posterior cingulate cortex; ROI, region of interest; SUV, standardized uptake value; SUVR, standardized uptake value ratio; WM, white matter.

*$P < .006$.

†$P < .001$.

‡$P < .0001$

§$P < .00001$ (statistically significant after Bonferroni correction over 8 regions).

alternative reference regions were visually similar. Voxel-wise analyses revealed that the CBF was significantly reduced in the precuneus/PCC area of both patients with aMCI and those with AD dementia compared with HCs ($P < .05$ corrected for age and education, cluster extent ≥ 50 voxels) (Fig. 3). Other regions of significant CBF reduction included the frontal and parietotemporal lobe and the hippocampus. Remarkably, eAV45 SUVR underestimated CBF reductions compared with R1 and was less closely related to FDG patterns (Figs. 2 and 3). The eAV45 and R1 reductions with a WM reference followed better the disease progression than with a CB reference region (Fig. 3A vs. 3B). Based on the regional group comparisons, all CBF measures were significantly lower in both patients with aMCI and AD dementia than those in HCs in the PCC ($\sim -20\%$; Table 3 and Supplementary Table 2). FDG $SUVR_{pons}$ was additionally reduced in the hippocampus ($\beta = -0.36$, $P = .03$) and precuneus ($\beta = -0.45$, $P = .02$) in patients with AD dementia, whereas $R1_{WM}$ showed a trend ($\beta = -0.29$ and -0.34, $P = .06$ and .08, respectively). eAV45 showed smaller effect size (i.e., standardized β) than R1, whereas FDG showed the highest effect sizes (Table 3).

Irrespective of CBF measure and reference region, reduced CBF in the PCC was significantly ($P < .025$) correlated with lower MMSE (Pearson r = 0.38–0.59) and delayed (Pearson r = 0.39–0.65) and immediate (Pearson r = 0.36–0.55) recall memory index scores (Table 4). The associations were most strongly driven by the aMCI and HC groups (Supplementary Fig. 2). In addition, there were significant associations between reduced MMSE and CBF in the precuneus when applying a WM reference region for eAV45 and R1 (Table 4). Correlation coefficients were weaker for eAV45 than for R1.

All CBF measures could discriminate between HCs and patients with aMCI in the PCC region (AUC = 0.84–0.88 [H_2O], 0.80–0.82 [FDG], 0.87–0.95 [eAV45], 0.86–0.95 [AV45-R1]), as well as between HCs and patients with AD dementia (AUC = 0.93–1.00 [H_2O], 0.92 [FDG], 0.84–0.90 [eAV45], 0.89–0.93 [AV45-R1]) (Supplementary Table 3). In addition, FDG $SUVR_{pons}$ could discriminate between HCs and patients with AD dementia in the frontal, temporal, and parietal lobe; precuneus; and hippocampus (AUC = 0.76–0.88). When the WM reference region was applied, the R1 and eAV45 measures could discriminate HCs from patients with aMCI and AD dementia also in the hippocampus (AUC = 0.73–0.87).

3.6. CBF proxies versus FDG PET

The optimal early time frame for eAV45 in relation to FDG SUVR was also 0–2 min (Supplementary Fig. 3). Both the early-phase (0–2 min) $SUVR_{CB}$ and $R1_{CB}$ of AV45 were strongly associated with FDG_{CB} (Pearson r ranging from 0.53 and 0.55 [occipital lobe] to 0.81 and 0.85 [hippocampus], respectively; $P < .001$) (Supplementary Table 4). Correlations between absolute measures were weaker.

4. Discussion

The present study showed that the FDG and AV45 (early-phase SUVR and SRTM2-based R1) indices were well correlated with the gold standard H_2O SUVR and may therefore serve as proxies of CBF. The within-subject correlations between R1 and eAV45 were likewise very high, indicating that the first 2 min of a dynamic AV45 scan—representing first-pass extraction of the tracer—can be representative for

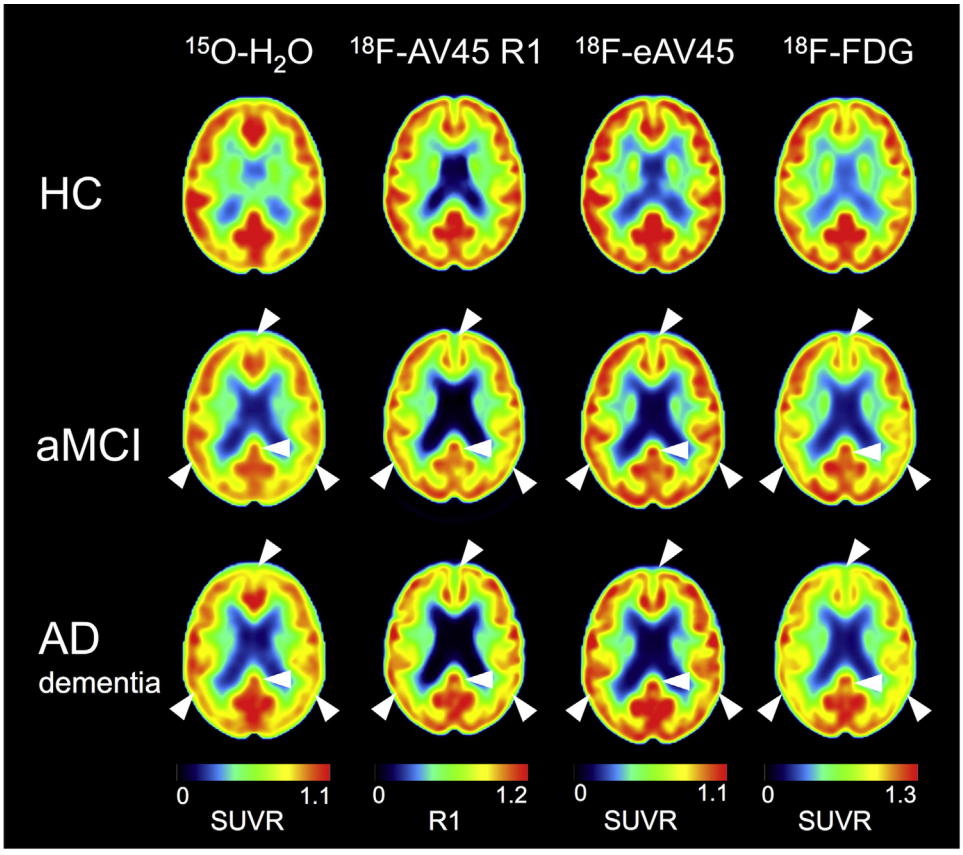

Fig. 2. Axial views of average spatially normalized H_2O SUVR, AV45-R1, eAV45 (0–2 min) SUVR and FDG SUVR images of the HC (n = 10), aMCI (n = 19), and AD dementia (n = 10) groups. A CB reference region was applied. White arrows indicate areas of visual blood flow reduction compared with HC, including frontal, parietotemporal, and precuneus/PCC area. Abbreviations: AD, Alzheimer's disease; aMCI, amnestic mild cognitive impairment; eAV45, early-phase AV45; HC, healthy control; PCC, posterior cingulate cortex; SUVR, standardized uptake value ratio.

perfusion. Both the early phases and R1 of AV45 are of clinical interest as amyloid-PET tracers benefit from the ability to provide information on both CBF (early phase) and Aβ burden (late phase) in one imaging session [12,24]. This may increase diagnostic accuracy and accelerate treatment initiation and clinical trial referral, while avoiding the increased radiation exposure and medical costs associated with an additional FDG scan. One may advocate that the use of eAV45 SUVR should be chosen over R1 because it avoids long dynamic scanning with labor-intensive kinetic modeling. However, in the present study, eAV45 SUVR tended to underestimate CBF reduction, was more weakly correlated to cognition, and showed lower discriminative ability in the hippocampus, precuneus, and PCC than R1. This may be related to a biased PET-to-MRI coregistration when using only the early-phase data compared with 60-min full-dynamic data. We suggest R1 as a more robust representation of CBF than the early phases.

This study reports for the first time associations between cognition and CBF in cases of sporadic AD using the gold standard measurement H_2O, with supporting data using R1, eAV45, and FDG. We found that reductions in all four measures were significantly correlated with lower MMSE and (immediate and delayed) memory index scores, but they were significant only in the PCC after correction for multiple comparisons and the covariates age and education. In addition, FDG and eAV45/$R1_{WM}$ showed significant correlations with MMSE in the precuneus. Previous studies have mainly focused on associations with MMSE and found significant results in the PCC/precuneus as well as in the parietotemporal association cortices [18,19,22,30]. With regard to discriminative ability, we found that all four CBF markers could significantly discriminate between HC and AD dementia in the PCC. In addition, FDG $SUVR_{pons}$ could discriminate in the frontal, parietotemporal, hippocampus, and precuneus areas. Other studies also found FDG to be slightly superior to other CBF markers in discriminating AD dementia or MCI Aβ+ from controls [20] and PiB+ from PiB- [12]. Distinct findings between CBF and CMRglc distribution markers might be explained by the fact that reduced uptake on FDG not only represents impaired CBF but also neuronal dysfunction. Although we and others have reported a significant overlap between both markers in the bilateral parietotemporal lobes, precuneus, and PCC [31], a regional neurovascular decoupling is present in the resting brain [32] as well as in the earlier

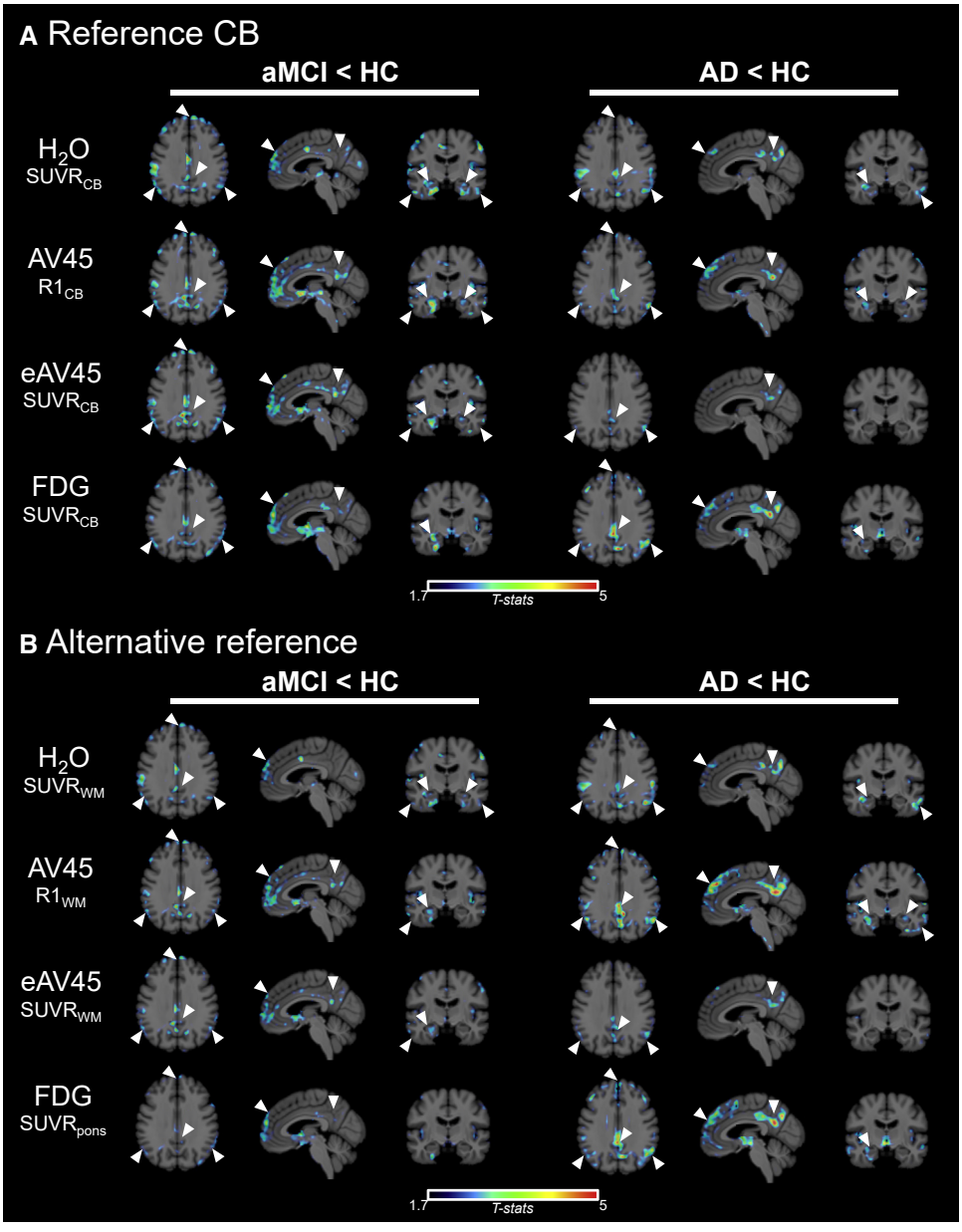

Fig. 3. T-maps showing significantly reduced CBF in aMCI ($n = 19$) and AD dementia ($n = 10$) versus HC ($n = 10$) in the frontal lobe, parietal lobe, precuneus/PCC (horizontal slice, white arrows); the frontal lobe, precuneus/PCC (sagittal slice, white arrows); the temporal lobe and hippocampus (coronal slice, white arrows). Panel (A) shows the results when CB normalization was applied, whereas panel (B) shows the results for alternative reference regions (i.e., WM for AV45 and H_2O, pons for FDG). A mask was applied around the ventricles because of spillover and enlargement of ventricles in aMCI/AD dementia. $P < .05$ corrected for age and education, cluster extent $\geq$50 voxels. Abbreviations: AD, Alzheimer's disease; aMCI, amnestic mild cognitive impairment; CB, cerebellar gray matter; CBF, cerebral blood flow; eAV45, early-phase AV45; HC, healthy control; PCC, posterior cingulate cortex; WM, white matter.

stages of disease progression [20,33]. We demonstrated that hypometabolic patterns extended over wider brain areas and became stronger with disease severity than patterns of hypoperfusion. Moreover, correlations between FDG and H_2O uptake values were region-dependent, being weak in the frontal and occipital lobe. Increased CBF in these regions has been hypothesized to reflect a vascular compensatory mechanism for reduced metabolism [34]. Therefore, although R1, eAV45, and FDG images can be used to represent tissue CBF, FDG remains the measure of choice for quantifying neuronal and synaptic function. Future studies should evaluate whether CBF proxies can replace FDG images on a single-subject level for clinical purposes, for example, to discriminate AD from non-AD dementias [21].

Head-to-head comparison between early-phase SUVR and R1 of AV45, in terms of regional correlation strength to FDG SUVR, showed similar results. Previous studies likewise compared R1 to the early phases of PiB [35,36] and AV45 [17] in relation to FDG, reporting comparable correlation strength and discriminative ability for both measures. Other literature has merely focused on the relationship between early-phase amyloid and FDG PET alone and reported

Table 3
Mean H2O, FDG, eAV45 SUVR, and AV45-R1 values (± standard deviation) and their differences between HC and AD dementia

	Hippocampus					Precuneus					PCC				
CBF measures	HC	AD	Δ (%)	β	*P*	HC	AD	Δ (%)	β	*P*	HC	AD	Δ (%)	β	*P*
Reference CB															
H_2O $SUVR_{CB}$	0.86 ± 0.1	0.87 ± 0.1	+1.2	0.17	.39	1.10 ± 0.1	1.04 ± 0.2	−5.5	−0.12	.59	**1.26 ± 0.1**	**0.98 ± 0.2**	**−22.2**	**−0.32**	**.04**
FDG $SUVR_{CB}$	0.72 ± 0.1	0.62 ± 0.1	−13.9	−0.26	.12	1.39 ± 0.1	1.26 ± 0.2	−9.4	−0.32	.12	**1.58 ± 0.1**	**1.33 ± 0.1**	**−15.8**	**−0.39**	**.03**
eAV45 $SUVR_{CB}$	0.72 ± 0.1	0.65 ± 0.1	−9.7	−0.15	.42	1.17 ± 0.1	1.11 ± 0.2	−5.1	−0.15	.47	**1.35 ± 0.1**	**1.15 ± 0.2**	**−14.8**	**−0.34**	**.03**
AV45-$R1_{CB}$	0.68 ± 0.1	0.60 ± 0.1	−11.8	−0.20	.26	1.15 ± 0.1	1.09 ± 0.2	−5.2	−0.20	.34	**1.34 ± 0.2**	**1.12 ± 0.1**	**−16.4**	**−0.36**	**.02**
Alternative reference															
H_2O $SUVR_{WM}$	1.58 ± 0.1	1.61 ± 0.2	+1.9	0.30	.13	2.03 ± 0.2	1.92 ± 0.2	−5.4	−0.07	.73	2.32 ± 0.1	1.86 ± 0.3	−19.8	−0.23	.13
FDG $SUVR_{pons}$	**1.09 ± 0.1**	**0.90 ± 0.1**	**−17.4**	**−0.36**	**.03**	**2.11 ± 0.2**	**1.83 ± 0.2**	**−13.3**	**−0.45**	**.02**	**2.40 ± 0.3**	**1.93 ± 0.2**	**−19.6**	**−0.45**	**.02**
eAV45 $SUVR_{WM}$	1.68 ± 0.2	1.46 ± 0.2	−13.1	−0.20	.20	2.72 ± 0.2	2.47 ± 0.3	−9.2	−0.26	.20	**3.16 ± 0.2**	**2.63 ± 0.4**	**−16.8**	**−0.32**	**.06**
AV45-$R1_{WM}$	**1.67 ± 0.2**	**1.41 ± 0.2**	**−15.6**	**−0.29**	**.06**	**2.82 ± 0.2**	**2.5 ± 0.2**	**−11.4**	**−0.34**	**.08**	**3.28 ± 0.2**	**2.65 ± 0.3**	**−19.2**	**−0.39**	**.02**

NOTE. for eAV45 SUVR, the 0–2 min frame was used (see Fig. 1). Target regions include hippocampus, precuneus, and PCC, and reference regions include either the CB or one of the alternative regions (WM for H_2O, eAV45, and R1; pons for FDG). Standardized βs (and *P* values) were based on ANCOVA, corrected for age and education, between diagnostic groups. Significant group differences are presented in bold typeface. In addition, FDG_{pons} was significantly reduced in the parietal lobe (β = −0.42, *P* = .04) and temporal lobe (β = −0.41, *P* = .05) in AD dementia compared with HCs.

Abbreviations: AD, Alzheimer's disease dementia; CB, cerebellar gray matter; CBF, cerebral blood flow; HC, healthy control; R1, AV45 relative delivery rate; PCC, posterior cingulate cortex; SUVR, standardized uptake value ratio; WM, white matter; Δ (%), percentage difference between average uptake in HC versus AD dementia.

good correlations (e.g., in PCC/parietal cortex, ePiB vs. FDG: r = 0.74 [12]; eFBB vs. FDG: r = 0.82–0.92 [21]; eAV45 vs. FDG: r = 0.80–0.86 [17]). The latter study by Hsiao et al. [17] suggested to extend the integration time from the first 2 min to the first 6 min to improve the associations with FDG. In contrast, we have shown that the 0- to 2-min interval for eAV45 was sufficient in comparison to both regional H_2O and FDG values. Discrepancies between both studies may arise from a different sample size (39 vs. 7 in the study by Hsiao et al. [17]) and partial-volume–corrected results (vs. noncorrected in the study by Hsiao et al. [17]). Furthermore, we found similar pattern of results in group contrast using all CBF measures except eAV45; therefore, we suggest R1 as a closer proxy of perfusion and synaptic function. These findings are in line with recent cross-sectional [37] and longitudinal [38] ^{11}C-PiB studies, comparing the early phases and R1 to FDG and/or H_2O PET. Nevertheless, compared with eAV45, R1 has the disadvantage of requiring a dynamic scanning protocol and would therefore only be advised in clinical research settings in which high accuracy is needed (e.g., longitudinal or therapy-monitoring studies). On the other hand, methods such as simultaneous ASL-MRI and amyloid-PET or pharmacokinetic modeling of a noninvasive dual-time-window acquisition (two short dynamic scans capturing respectively the peak [early phase] and the tail [late phase] without acquiring the central portion of the time-activity curve) could be investigated as simplified alternatives to R1 as well.

Table 4
Correlation (Pearson r) of H_2O, FDG SUVR, and AV45 (early-phase SUVR, R1) in the precuneus or PCC with cognitive score (MMSE, delayed and immediate recall index score)

	H_2O SUVR			FDG SUVR		eAV45 SUVR		AV45-R1	
ROI	CB	WM	Pons	CB	Pons	CB	WM	CB	WM
MMSE									
Precuneus	0.30	0.34	0.43*	0.41*	0.43*	0.28	0.42*	0.28	0.46*
PCC	0.38*	0.41*	0.44*	0.47†	0.46†	0.45*	0.52†	0.47†	0.59‡
Delayed memory									
Precuneus	0.18	0.17	0.25	0.29	0.34	0.17	0.25	0.20	0.32
PCC	0.44*	0.39*	0.44*	0.65§	0.62§	0.54†	0.55‡	0.58‡	0.65§
Immediate memory									
Precuneus	0.20	0.04	0.26	0.40*	0.29	0.27	0.23	0.30	0.27
PCC	0.49†	0.40*	0.48†	0.45*	0.36*	0.48†	0.40*	0.55‡	0.48†

NOTE. CB, pons, and WM were investigated as reference regions.

Abbreviations: CB, cerebellar gray matter; eAV45, early-phase AV45; MMSE, Mini-Mental State Examination; R1, AV45 relative delivery rate; PCC, posterior cingulate cortex; ROI, region of interest; SUVR, standardized uptake value ratio; WM, white matter.

*$P < .025$.

†$P < .005$.

‡$P < .0005$.

§$P < .00005$ (partial correlations corrected for age, education, and multiple comparisons via Bonferroni over 2 regions).

Within-subject correlative analyses and intergroup voxel-wise analyses were dependent on reference region selection. CB was used as a reference region in this study because of its low susceptibility to age-related atrophy and changes in metabolism and CBF [39,40]. WM was applied as an alternative reference region for (early-phase and R1) AV45 measures, as recent studies have shown its use in accurately quantifying Aβ plaque load [14]. On the other hand, for FDG PET, we selected the pons as an alternative reference region based on previous literature [41]. To the best of our knowledge, this is the first study investigating different reference regions for FDG, eAV45, and R1 in relation to H_2O data. First, we found that SRTM2-based R1 was more strongly correlated to the reference standard 2TCM-based R1 when using CB instead of WM as the reference

region. This might be explained by a significant ($P < .0001$) greater violation of one of the SRTM2 assumptions when WM normalization was applied, namely that the nonspecific K1/k2 in the target should equal the (nonspecific) V_T in the reference, assuming both regions fit a 2TCM. In line with this, $R1_{CB}$ was more strongly associated to H_2O SUVR than $R1_{WM}$. Second, in relation to disease severity, aMCI but not AD dementia showed the strongest reduction in perfusion compared with HC, both for eAV45 SUVR and R1 normalized to CB. When using a WM reference region instead, perfusion was the lowest in AD dementia as should be expected given the progression of disease. This discrepancy might be explained by a reduced blood flow in the CB of AD dementia compared with HC and MCI [14], questioning its use as a reference region. Moreover, $R1_{WM}$ was correlated stronger to cognitive impairment in the PCC and precuneus than $R1_{CB}$. Hence, WM normalization resulted in better correspondence of CBF patterns with disease severity. This is in line with recent amyloid-PET studies reporting more stable and more plausible (e.g., nondecreasing) longitudinal SUVR values when the reference region included WM [42,43].

Noteworthy is that CBF was measured with ^{15}O-H_2O PET as the gold standard. Owing to its limited blood-brain barrier permeability (extraction factor ≈ 90–95%), ^{15}O-H_2O PET may underestimate the true absolute CBF at elevated flow rates compared with the resting brain (>55 ml/min/100g) [44]. Another limitation of the study includes the relatively small sample size, which did not allow performing a multiple comparison correction at the voxel level. However, the main goal of this study was to compare correlation findings among PET modalities rather than to establish correlation patterns. Finally, different CBF PET modalities were not consistently recorded on the same day within one subject. Therefore, daily fluctuations in global CBF might explain why within-subject correlations between the absolute CBF measures were weaker than those between the relative measures.

5. Conclusion

The present study showed that the FDG and AV45 (early-phase [0–2 min] SUVR and SRTM2-based R1) indices were well correlated with the gold standard H_2O PET and may therefore serve as surrogate markers of CBF. In addition, we showed that all CBF measures were significantly reduced in the PCC of aMCI and AD dementia subjects and that these reductions were significantly associated with reduced cognitive scores. Both R1 and the early phases of AV45 are of clinical interest in case one wants to combine perfusion and Aβ pathological information in one imaging session. Our study showed that R1 (especially using a WM reference region) better reflected the disease severity than did early-phase AV45 but has the disadvantage that a dynamic PET scan with pharmacokinetic modeling is required.

Acknowledgments

The authors acknowledge Charisse Somers, Hanne Struyfs, Femke Soetewey, Tobi Van den Bossche, and Sara Van Mossevelde for their help with the recruitment and clinical characterization of the subjects included. They would also like to thank Margaretha Miedema and Clara De Puydt for help with the data processing.

Funding sources: This study was in part funded by IWT TGO BIOADAPTAD and by the University of Antwerp and its University Hospital, under grant agreement n° 120835 A14/0161; University Hospital Antwerp; the University of Antwerp Research Fund; the Institute Born-Bunge (IBB, www.bornbunge.be); and the Flanders Impulse Program on Networks for Dementia Research (VIND).

Supplementary data

Supplementary data related to this article can be found at https://doi.org/10.1016/j.jalz.2019.05.010.

RESEARCH IN CONTEXT

1. Systematic review: This cross-sectional study validated the use of ^{18}F-FDG PET, the early phases (first 2 min) and the delivery rate R1 of ^{18}F-AV45 PET as surrogate markers of cerebral blood flow, based on their strong association to the gold standard ^{15}O-H_2O PET. ^{18}F-FDG and R1 were more sensitive markers to reflect the disease severity than early-phase ^{18}F-AV45 PET.
2. Interpretation: Our results suggest that clinical trial and research studies for which high accuracy is needed (e.g., therapy-monitoring studies) may use a single dynamic ^{18}F-AV45 PET scan to accurately retrieve perfusion information (R1) in addition to amyloid-β information. Furthermore, a decoupling between flow and metabolism is present, which seems dependent on region as well as clinical diagnosis.
3. Future directions: Given the possible application of dual-biomarker PET, future studies should investigate the ability of the cerebral blood flow proxies to replace ^{18}F-FDG images on a single-subject level for clinical purposes.

References

[1] Braak H, Braak E. Neuropathological stageing of Alzheimer-related changes. Acta Neuropathol 1991;82:239–59.

[2] Rius-Pérez S, Tormos AM, Pérez S, Taléns-Visconti R. Vascular pathology: cause or effect in Alzheimer's disease? Neurology 2017; 33:112–20.
[3] Binnewijzend MAA, Benedictus MR, Kuijer JPA, van der Flier WM, Teunissen CE, Prins ND, et al. Cerebral perfusion in the predementia stages of Alzheimer's disease. Eur Radiol 2016;26:506–14.
[4] Mosconi L, Berti V, Glodzik L, Pupi A, De Santi S, de Leon MJ. Preclinical detection of Alzheimer's disease using FDG-PET, with or without amyloid imaging. J Alzheimers Dis 2010;20:843–54.
[5] Hirao K, Ohnishi T, Hirata Y, Yamashita F, Mori T, Moriguchi Y, et al. The prediction of rapid conversion to Alzheimer's disease in mild cognitive impairment using regional cerebral blood flow SPECT. Neuroimage 2005;28:1014–21.
[6] Benedictus MR, Leeuwis AE, Binnewijzend MAA, Kuijer JPA, Scheltens P, Barkhof F, et al. Lower cerebral blood flow is associated with faster cognitive decline in Alzheimer. Eur Radiol 2017; 27:1169–75.
[7] Leeuwis AE, Benedictus MR, Kuijer JPA, Binnewijzend MAA, Hooghiemstra AM, Verfaillie SCJ, et al. Lower cerebral blood flow is associated with impairment in multiple cognitive domains in Alzheimer's disease. Alzheimers Dement 2017;13:531–40.
[8] Leijenaar JF, van Maurik IS, Kuijer JPA, van der Flier WM, Scheltens P, Barkhof F, et al. Lower cerebral blood flow in subjects with Alzheimer's dementia, mild cognitive impairment, and subjective cognitive decline using two-dimensional phase-contrast magnetic resonance imaging. Alzheimers Dement 2017;9:76–83.
[9] Herscovitch P, Markham J, Raichle ME. Brain Blood Flow Measured with Intravenous H2-15O. I. Theory and Error Analysis. J Nucl Med 1983;24:782–9.
[10] Blomquist G, Engler H, Nordberg A, Ringheim A, Wall A, Forsberg A, et al. Unidirectional influx and net accumulation of PIB. Open Neuroimag J 2008;2:114–25.
[11] Chen YJ, Rosario BL, Mowrey W, Laymon CM, Lu X, Lopez OL, et al. Relative 11C-PiB delivery as a proxy of relative CBF: Quantitative evaluation using single-session 15O-water and 11C-PiB PET. J Nucl Med 2015;56:1199–205.
[12] Forsberg A, Engler H, Blomquist G, Långström B, Nordberg A. The use of PIB-PET as a dual pathological and functional biomarker in AD. Biochim Biophys Acta 2012;1822:380–5.
[13] Lammertsma AA, Hume SP. Simplified reference tissue model for PET receptor studies. Neuroimage 1996;4:153–8.
[14] Ottoy J, Verhaeghe J, Niemantsverdriet E, Wyffels L, Somers C, De Roeck E, et al. Validation of the semiquantitative static SUVR method for 18F-AV45 PET by pharmacokinetic modeling with an arterial input function. J Nucl Med 2017;58:1483–9.
[15] Arakawa Y, Nai Y, Shidahara M, Furumoto S, Seki C, Okamura N, et al. Prediction of the clinical SUV ratio in amyloid PET imaging using a biomathematic modeling approach toward the efficient development of a radioligand. J Nucl Med 2017;58:1285–92.
[16] Wu Y, Carson RE. Noise reduction in the simplified reference tissue model for neuroreceptor functional imaging. J Cereb Blood Flow Metab 2002;22:1440–52.
[17] Hsiao I-T, Huang C-C, Hsieh C-J, Hsu W-C, Wey S-P, Yen T-C, et al. Correlation of early-phase 18F-florbetapir (AV-45/Amyvid) PET images to FDG images: preliminary studies. Eur J Nucl Med Mol Imaging 2012;39:613–20.
[18] Rostomian AH, Madison C, Rabinovici GD, Jagust WJ. Early 11C-PIB frames and 18F-FDG PET measures are comparable: a study validated in a cohort of AD and FTLD patients. J Nucl Med 2011; 52:173–9.
[19] Meyer PT, Hellwig S, Amtage F, Rottenburger C, Sahm U, Reuland P, et al. Dual-biomarker imaging of regional cerebral amyloid load and neuronal activity in dementia with PET and 11C-labeled Pittsburgh compound B. J Nucl Med 2011;52:393–400.
[20] Rodriguez-Vieitez E, Carter SF, Chiotis K, Saint-Aubert L, Leuzy A, Scholl M, et al. Comparison of early-phase 11C-deuterium-L-deprenyl and 11C-Pittsburgh compound B PET for assessing brain perfusion in Alzheimer disease. J Nucl Med 2016;57:1071–7.
[21] Daerr S, Brendel M, Zach C, Mille E, Schilling D, Zacherl MJ, et al. Evaluation of early-phase [18F]-florbetaben PET acquisition in clinical routine cases. Neuroimage Clin 2016;14:77–86.
[22] Tiepolt S, Hesse S, Patt M, Luthardt J, Schroeter ML, Hoffmann K-T, et al. Early [18F]florbetaben and [11C]PiB PET images are a surrogate biomarker of neuronal injury in Alzheimer's disease. Eur J Nucl Med Mol Imaging 2016;43:1700–9.
[23] Fu L, Liu L, Zhang J, Xu B, Fan Y, Tian J. Comparison of dual-biomarker PIB-PET and dual-tracer PET in AD diagnosis. Eur Radiol 2014;24:2800–9.
[24] Lin K-J, Hsiao I-T, Hsu J-L, Huang C-C, Huang K-L, Hsieh C-J, et al. Imaging characteristic of dual-phase 18F-florbetapir (AV-45/Amyvid) PET for the concomitant detection of perfusion deficits and beta-amyloid deposition in Alzheimer's disease and mild cognitive impairment. Eur J Nucl Med Mol Imaging 2016;43:1304–14.
[25] Duff K, Humphreys Clark JD, O'Bryant SE, Mold JW, Schiffer RB, Sutker PB. Utility of the RBANS in detecting cognitive impairment associated with Alzheimer's disease: sensitivity, specificity, and positive and negative predictive powers. Arch Clin Neuropsychol 2008; 23:603–12.
[26] McKhann GM, Knopman DS, Chertkow H, Hyman BT, Jack CR Jr, Kawas CH, et al. The diagnosis of dementia due to Alzheimer's disease: recommendations from the National Institute on Aging-Alzheimer's Association workgroups on diagnostic guidelines for Alzheimer's disease. Alzheimers Dement 2011;7:263–9.
[27] Albert MS, DeKosky ST, Dickson D, Dubois B, Feldman HH, Fox NC, et al. The diagnosis of mild cognitive impairment due to Alzheimer's disease: Recommendations from the National Institute on Aging-Alzheimer's Association workgroups on diagnostic guidelines for Alzheimer's disease. Alzheimers Dement 2011; 7:270–9.
[28] Niemantsverdriet E, Ottoy J, Somers C, De Roeck E, Struyfs H, Soetewey F, et al. The cerebrospinal fluid Aβ1–42/Aβ1–40 ratio improves concordance with amyloid-PET for diagnosing Alzheimer's disease in a clinical setting. J Alzheimers Dis 2017; 60:561–76.
[29] Rousset OG, Ma Y, Evans AC. Correction for partial volume effects in PET: principle and validation. J Nucl Med 1998;39:904–11.
[30] Kaneta T, Katsuse O, Hirano T, Ogawa M, Shihikura-Hino A, Yoshida K, et al. Voxel-wise correlations between cognition and cerebral blood flow using arterial spin-labeled perfusion MRI in patients with Alzheimer's disease: a cross-sectional study. BMC Neurol 2017;17:91.
[31] Chen Y, Wolk DA, Reddin JS, Korczykowski M, Martinez PM, Musiek ES, et al. Voxel-level comparison of arterial spin-labeled perfusion MRI and FDG-PET in Alzheimer disease. Neurology 2011;77:1977–85.
[32] Gur RC, Ragland JD, Reivich M, Greenberg JH, Alavi A, Gur RE. Regional differences in the coupling between resting cerebral blood flow and metabolism may indicate action preparedness as a default state. Cereb Cortex 2009;19:375–82.
[33] Yan L, Liu CY, Wong K-P, Huang S-C, Mack WJ, Jann K, et al. Regional association of pCASL-MRI with FDG-PET and PiB-PET in people at risk for autosomal dominant Alzheimer's disease. Neuroimage Clin 2018;17:751–60.
[34] Wierenga CE, Hays CC, Zlatar ZZ. Cerebral blood flow measured by arterial spin labeling MRI as a preclinical marker of Alzheimer's disease. J Alzheimers Dis 2014;42:S411–9.
[35] Rodriguez-Vieitez E, Leuzy A, Chiotis K, Saint-Aubert L, Wall A, Nordberg A. Comparability of [18F]THK5317 and [11C]PIB blood flow proxy images with [18F]FDG positron emission tomography in Alzheimer's disease. J Cereb Blood Flow Metab 2017;37:740–9.
[36] Oliveira FPM, Moreira AP, de Mendonça A, Verdelho A, Xavier C, Barroca D, et al. Can 11C-PiB-PET relative delivery R1 or 11C-

PiB-PET perfusion replace 18F-FDG-PET in the assessment of brain neurodegeneration? J Alzheimers Dis 2018;65:89–97.

[37] Joseph-Mathurin N, Su Y, Blazey TM, Jasielec M, Vlassenko A, Friedrichsen K, et al. Utility of perfusion PET measures to assess neuronal injury in Alzheimer's disease. Alzheimers Dement 2018; 10:669–77.

[38] Bilgel M, Beason-Held L, An Y, Zhou Y, Wong DF, Resnick SM. Longitudinal evaluation of surrogates of regional cerebral blood flow computed from dynamic amyloid PET imaging. J Cereb Blood Flow Metab 2019 Feb 12 [Epub ahead of print]. https://doi.org/10.1177/0271678X19830537.

[39] Bauer CM, Cabral HJ, Greve DN, Killiany RJ. Differentiating between normal aging, mild cognitive impairment, and Alzheimer's disease with FDG-PET: effects of normalization region and partial volume correction method. J Alzheimers Dis Parkinsonism 2013;3:1.

[40] Marchal G, Rioux P, Petit-Taboué MC, Sette G, Travère JM, Le Poec C, et al. Regional cerebral oxygen consumption, blood flow, and blood volume in healthy human aging. Arch Neurol 1992; 49:1013–20.

[41] Minoshima S, Frey KA, Foster NL, Kuhl DE. Preserved pontine glucose metabolism in Alzheimer disease: a reference region for functional brain image (PET) analysis. J Comput Assist Tomogr 1995; 19:541–7.

[42] Landau SM. Optimizing longitudinal β-amyloid PET measurement: the challenges of intensity normalization. J Nucl Med 2018; 59:1581–2.

[43] Ottoy J, Niemantsverdriet E, Verhaeghe J, De Roeck E, Struyfs H, Somers C, et al. Association of short-term cognitive decline and MCI-to-AD dementia conversion with CSF, MRI, amyloid- and 18F-FDG-PET imaging. Neuroimage Clin 2019; 22:101771.

[44] Raichle ME, Martin W, Herscovitch P, Mintun MA, Markham J. Brain blood flow measured with intravenous 15O-H20. II. Implementation and validation. J Nucl Med 1983;24:790–8.